FINITE AMPLITUDE TIDAL SANDBANKS. ONE-DIMENSIONAL EQUILIBRIUM PROFILES

Pieter C. Roos[1], Suzanne J. M. H. Hulscher[2], Ruud M. J. van Damme[3]

Abstract: We investigate tidal sandbanks with a nonlinear morphodynamic model. The model consists of shallow water flow (including Coriolis and friction effects), bedload and suspended load transport to describe the sea bed evolution. We look into the finite amplitude behaviour of sandbanks with preferred spacing and orientation from linear theory. In case of a suspended load sediment transport formulation, this leads to equilibrium profiles, which express a balance between drag effects and slope effects on sediment transport. For a bedload transport formulation the sea bed develops into an unrealistic pattern with sharp crests that tend to touch the water surface. The stability properties of the suspended load equilibrium differ from those of a flat bed. We discuss the implications of these results for the understanding of sandbanks as well as the modelling of human intervention at the sea bed, such as large-scale offshore sand extraction.

INTRODUCTION

Shallow shelf seas like the North Sea exhibit several types of rhythmic features. With a wavelength of several kilometers and a height up to 80% of the water depth (Idier and Astruc, 2001), *tidal sandbanks* are clearly the largest of these offshore bedforms (see Dyer and Huntley 1999, who refer to these features as *open shelf ridges*). Their crest orientation is usually counterclockwise with respect to the tidal current. Sea users benefit from a better understanding of sandbank dynamics, making it a practically relevant subject of research. An example of such sea use is offshore sand extraction, possibly carried out in areas where sandbank patterns occur. In fact, dredging from the banks themselves seems an attractive option. Due to increasing demand, future sandpits off the Dutch coast are likely to be of the order of 10^8 m^3 (Peters, 2001).

[1]Water Engineering and Management, Faculty of Engineering Technology, University of Twente, P.O. Box 217, 7500 AE Enschede, The Netherlands. p.c.roos@ctw.utwente.nl

[2]Water Engineering and Management, Faculty of Engineering Technology, University of Twente, P.O. Box 217, 7500 AE Enschede, The Netherlands. s.j.m.h.hulscher@ctw.utwente.nl

[3]Faculty of Mathematical Sciences, University of Twente, P.O. Box 217, 7500 AE Enschede, The Netherlands. r.m.j.vandamme@math.utwente.nl

For a pit depth of a few meters, this corresponds to horizontal dimensions of several kilometers, i.e. of the order of the spacing of tidal sandbanks. Predicting the long-term fate of such a pit requires insight in the dynamics of tidal sandbanks.

Much of the research on tidal sandbanks has focused on the process of *formation* from a process-based point of view. Huthnance (1982a) was the first to show that tidal sandbanks may form as an inherent instability of a flat sea bed subject to tidal motion. In doing so, he used a morphodynamic model, that was later extended by De Vriend (1990) and Hulscher et al. (1993). It consists of shallow-water flow and sediment transport (usually a parametrization of bedload transport), as a result of which the sea bed evolves. Then, a linear stability analysis shows that there are wavy perturbations, so-called modes, against which the flat sea bed is unstable. The hydrodynamical mechanisms behind this positive feedback mechanism are friction-topography and Coriolis-topography interactions (see Zimmerman 1981, Pattiaratchi and Collins 1987 or the review by Dyer and Huntley 1999). The mode that grows fastest predicts the bank wavelength as well as its orientation with respect to the principal direction of the tidal current. This linear analysis is valid only in the initial stage of formation, when bed amplitudes are still small (compared to the water depth). Describing the subsequent growth requires a nonlinear analysis.

Only few (process-based) models have been developed to describe nonlinear sandbank dynamics. Huthnance (1982a) numerically obtained equilibrium profiles for bedload transport. More recently, Idier and Astruc (2001) reproduced the (analytically obtained) growth characteristics from linear theory with a fully numerical approach (bedload transport). Furthermore, they used an initial bed response analysis to estimate saturation bank height (for purely sinusoidal profiles and steady current). They found that banks lower than 94% of the water depth initially tend to grow, and those higher tend to decay.

In this paper we consider a morphodynamic model similar to that by Huthnance (1982a). However, our approach will be somewhat different as we will look into the role of the sediment transport formulation. We consider two sediment transport formulations. The first, commonly used to model bedload transport (e.g. by Huthnance 1982a, Hulscher et al. 1993), does not contain a spatial lag. The other, commonly used to model suspended load transport, does contain a spatial lag effect. As it turns out, this lag effect is a prerequisite to find equilibrium sandbank profiles. Furthermore, our treatment of the spatially independent part of the hydrodynamics (the so-called ($k=0$)-mode) differs from the one by Huthnance (1982a). We investigate the characteristics of the equilibrium shapes along with the underlying physical mechanisms.

THE MODEL

Hydrodynamics

We first present the model in dimensionless form. An extensive description of the scaling procedure can be found in Hulscher et al. (1993). Consider an offshore part of a shallow shelf sea with free surface at $z = \zeta$ and the sea bed at $z = -1 + h$ (see figure 1; vertical coordinate scaled against the mean water depth, typically some 20-30 m). Let $\boldsymbol{u} \equiv (u, v)$ denote the depth-averaged flow velocity with components u and v

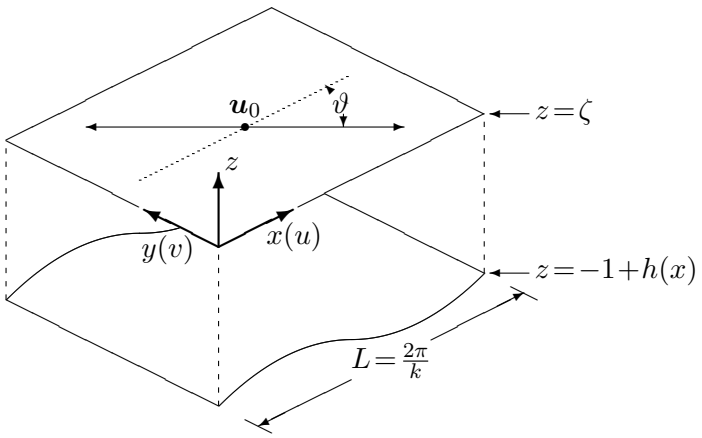

Figure 1: Definition sketch of the model geometry.

(scaled against maximum tidal velocity, typically 1 m s^{-1}) in the horizontal directions x and y (scaled against tidal excursion length), respectively. For sake of convenience, we restrict to topographies that are uniform in one horizontal direction, i.e. we assume that h is a function of x only. This is justified by the rather large width to spacing ratio of tidal sandbanks. The depth-averaged shallow-water equations then reduce to

$$F_x + \frac{\partial \zeta}{\partial x} + u\frac{\partial u}{\partial x} - fv + \frac{ru}{1-h} = 0, \tag{1a}$$

$$F_y + u\frac{\partial v}{\partial x} + fu + \frac{rv}{1-h} = 0, \tag{1b}$$

$$\frac{\partial}{\partial x}\left[(1-h)u\right] = 0. \tag{1c}$$

Here, f is a Coriolis parameter and r a linear friction coefficient. We have adopted a rigid-lid approach, effectively treating ζ as a pressure at the surface. Furthermore, we ignore acceleration terms in the momentum equations. The system is driven by a tidal forcing $\boldsymbol{F} \equiv (F_x, F_y)$, which can be looked upon as a time-varying pressure gradient. In the continuity equation (1c), we neglect the depth changes on the tidal time scale. Values of the parameters are taken from Hulscher et al. (1993): $f = 0.83$, $r = 0.6$.

Sediment transport

We assume that the sea bed consists of noncohesive sediment of uniform size. Let $\boldsymbol{q} \equiv (q_x, q_y)$ denote the (scaled) volumetric bedload sediment flux, the divergences of which determine the bed evolution. Owing to the uniformity in y-direction, only the x-component of the bedload flux contributes to the bed evolution. It is parametrized as a function of the depth-averaged flow velocity $\boldsymbol{u}$ and the local bed slope $\partial h/\partial x$ (see Van Rijn, 1993), according to

$$q_x = \alpha|\boldsymbol{u}|^\beta \left(\frac{u}{|\boldsymbol{u}|} - \lambda\frac{\partial h}{\partial x}\right). \tag{2}$$

Different parameters appear: a proportionality factor α (also accounting for bed porosity), a velocity power β and a bedslope coefficient λ. For suspended load transport we

use an advection equation (see Schuttelaars, 1997)

$$\gamma \frac{\partial (cu)}{\partial x} = c_e - c, \qquad \text{with} \quad c_e = \alpha |\boldsymbol{u}|^{\beta - 1}. \tag{3a,b}$$

Here, c is the (scaled) *depth-integrated* sediment concentration, i.e. the amount of suspended matter in the water column. Furthermore, γ is a spatial relaxation parameter, related to settling velocity and therefore dependent on grain size (Van Rijn, 1993). We neglect the temporal relaxation. The right-hand side of (3a) represents the entrainment and deposition of sediment in suspension, the former modelled as a power $(\beta - 1)$ of the depth-averaged flow velocity with a proportionality factor α (also accounting for bed porosity), the latter proportional to the local sediment concentration. Typical parameter values are: $\alpha = 0.5 \cdot 10^{-6} - 0.5 \cdot 10^{-5}$, $\beta = 3$ and $\lambda = 0.0084$ (see Hulscher et al. 1993 for bedload, Dyer and Soulsby 1988 for suspended load). In (2) and (3) we neglect the threshold for sediment transport.

Bed evolution

We adopt a multiple time scale analysis with a fast hydrodynamic time t and a slow morphodynamic time τ. The flow and sediment transport evolve on both t and τ, whereas the sea bed is assumed to evolve on τ only. This effectively decouples the flow and sediment transport module from the sea bed evolution module. The bed evolves as a result of (tidally averaged) divergences in the bedload sediment flux and the net difference between entrainment and deposition of sediment in suspension, i.e.

$$\frac{\partial h}{\partial \tau} = \begin{cases} -\dfrac{\partial \langle q_x \rangle}{\partial x} & \text{for bedload,} \\ \dfrac{\langle c - c_e \rangle}{\gamma} + \lambda \dfrac{\partial^2 h}{\partial x^2} & \text{for suspended load.} \end{cases} \tag{4}$$

in case of bedload or suspended load transport. Here, the angle brackets $\langle \cdot \rangle$ denote averaging over a tidal cycle. Also the suspended load formulation includes a bedslope effect, with coefficient λ. Finally, the slow time is defined by $\tau = \alpha t$ and $\tau = 1$ corresponds to a dimensional time of the order of $50 - 500$ years.

Basic state and expansion

Let $\phi \equiv (h, u, v, \zeta, q_x, c)$ denote the state of the system. The model allows for a simple solution ϕ_0, called the *basic state*, which describes an arbitrary yet spatially uniform flow over a flat sea bed $h \equiv 0$. We choose our coordinate system such that the forcing $\boldsymbol{F} \equiv (F_x, F_y)$ induces a basic flow, inclined at an angle ϑ with respect to the x-axis, i.e.

$$\boldsymbol{u}_0 \equiv (u_0, v_0) = I(t)(\cos \vartheta, -\sin \vartheta), \tag{5a}$$

in which the time-dependency is that of a symmetric *block flow*, given by

$$I(t) = \begin{cases} 1 & 0 \le t < \pi, \\ -1 & \pi \le t < 2\pi. \end{cases} \tag{5b}$$

Note that time has been scaled such that the interval $t = [0, 2\pi]$ covers an M_2-cycle of 12h25'. The rather simplified flow representation (5) allows us to *mimic* a symmetric

tidal flow at low computational cost. As we have neglected inertial terms in the model equations the tidal average simply reduces to the weighted average of two steady states, one with $I = 1$, the other with $I = -1$, both with a weighting coefficient $1/2$. The sea bed of the basic state remains flat as the righthand side of (4) vanishes. The basic state serves as the reference solution for both the linear and the nonlinear analysis. We therefore consider the state of the system relative to this basic state, by expanding according to

$$\phi = \phi_0 + \phi'. \tag{6}$$

In the linear analysis we require the so-called *perturbed state* ϕ' to be so small, that we may discard the terms nonlinear in ϕ'. For the nonlinear analysis, no such restriction exists.

LINEAR THEORY: ONSET OF FORMATION

As initial topography, we introduce a wavy perturbation of the flat sea bed

$$h' = \epsilon \mathrm{e}^{\mathrm{i}kx} + c.c. \qquad \text{at } \tau = 0. \tag{7}$$

The perturbation is characterized by (k, ϑ), i.e. the wavenumber and its orientation with respect to the basic flow (see figure 1). Negative ϑ-values correspond to a cyclonic crest orientation, positive ϑ-values to an anticyclonic crest orientation (Northern Hemisphere). Moreover, *c.c.* denotes the complex conjugation. The initial bed amplitude is assumed to be infinitesimally small ($\epsilon \ll 1$). In order to calculate the system's response to (7), we insert the expansion (6) into the model equations. We then arrive at a set of equations for the perturbed state ϕ', for which we write

$$\phi' = \Phi' \mathrm{e}^{\mathrm{i}kx} + c.c. \tag{8}$$

with Fourier components $\Phi' = \epsilon(H', U', V', Z', Q', C')$ where $H' = 1$ at $\tau = 0$. We discard the nonlinear terms in ϕ', i.e. those pertaining to second and higher powers of ϵ. The expressions for the components of Φ' are given in the Appendix. The linear analysis predicts $\partial H'/\partial\tau = \omega H'$, i.e. exponential growth or decay of the wavy feature, according to

$$h' = \epsilon \mathrm{e}^{\omega\tau} \mathrm{e}^{\mathrm{i}kx} + c.c. \tag{9}$$

Here $\omega = \omega_r + \mathrm{i}\omega_i$ is the *growth rate*, a complex number which depends on the perturbation characteristics (k, ϑ) and the set of physical parameters. Its real part ω_r is related to the amplitude growth (or decay) of the perturbation, whereas its imaginary part ω_i is associated with migration. However, for the symmetric basic flow considered here, the imaginary part vanishes. Expressions for the growth rate ω are given in the Appendix. The mode $(k_\mathrm{F}, \vartheta_\mathrm{F})$ for which the real part ω_r of the growth rate is maximal is called the *fastest growing mode*. This mode will emerge initially from an arbitrarily perturbed flat bed. The wavelength $L_F \equiv 2\pi/k_\mathrm{F}$ and orientation of the fastest growing mode turn out to agree well with those of sandbanks in the North Sea (see Huthnance 1982a, Hulscher et al. 1993). Typical growth rate plots are given in figure 2). In the linear analysis, bedload transport turns out to be a limiting case of suspended load transport for vanishing γ, i.e. $\lim_{\gamma\downarrow 0} \omega_\mathrm{susp} = \omega_\mathrm{bed}$ (see Appendix).

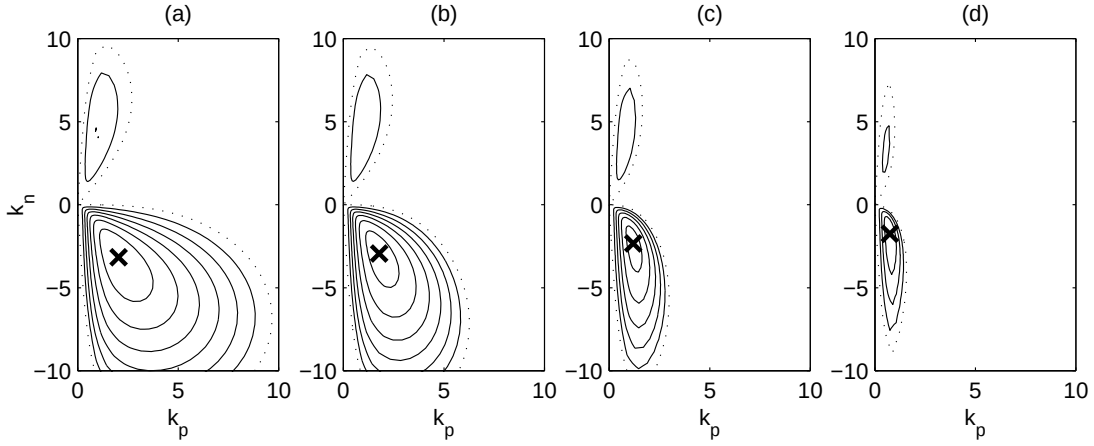

Figure 2: Contour plot of growth rates as a function of $k_p \equiv k\cos\vartheta$ and $k_n \equiv k\sin\vartheta$. Solid contours correspond to amplification ($\omega_r > 0$), the marginal contour ($\omega_r = 0$) is dotted and the fastest growing mode is denoted by a cross. (a) Bedload transport, (b-d) suspended load transport for three values of the relaxation parameter γ: (b) $\gamma = 0.01$, (c) $\gamma = 0.1$ and (d) $\gamma = 0.5$. Other parameters set at $f = 0.83$, $r = 0.6$, $\beta = 3$, $\lambda = 0.0084$. (We did not plot the halfplane where $k_p < 0$, as it follows immediately from the point symmetry about the origin. Perturbations with wave numbers k and $-k$ are identical.)

FINITE AMPLITUDE THEORY: SUBSEQUENT GROWTH

Expansion and initial topography

Starting point of the nonlinear analysis is the fastest growing mode obtained from the linear analysis. We investigate how this mode develops in the finite amplitude regime, where the expansion (8) is no longer appropriate as nonlinear effects generate higher harmonics. To that end, we set $\vartheta = \vartheta_{\mathrm{F}}$ and consider the state as a Fourier series containing the wavenumbers $k = 0$, $k = k_{\mathrm{F}}$ and a finite number of higher harmonics (see figure 3):

$$\phi' = \sum_{m=-M}^{M} \Phi'_m \mathrm{e}^{\mathrm{i}k_{\mathrm{F}}mx}. \tag{10}$$

Here M is the highest mode number and the Fourier components are denoted by $\Phi'_m = (H'_m, U'_m, V'_m, Z'_m, Q'_m, C'_m)$. The variables must be real quantities, so $\Phi'_{-m} = \overline{\Phi'_m}$ (an overbar denotes the complex conjugation). For each higher harmonic involved we let ω_m denote the growth rate from linear theory. Note that (10) is an expansion in eigenfunctions of the linear system. In this study we do not include subharmonics, i.e. we do not consider wavenumbers smaller than k_{F}. As initial topography, we take (7) but drop the restriction of an infinitesimally small bed amplitude: we now allow $|\epsilon| < 1$. However, any topography of the form (10) with $h' < 1$ can serve as initial condition.

Hydrodynamics and sediment transport

For a given topography, the derivation of the cross-bank velocity u is mainly governed by the continuity equation (1c), which immediately leads to

$$u \equiv u_0 + u' = \frac{\xi u_0}{1 - h'}, \tag{11a}$$

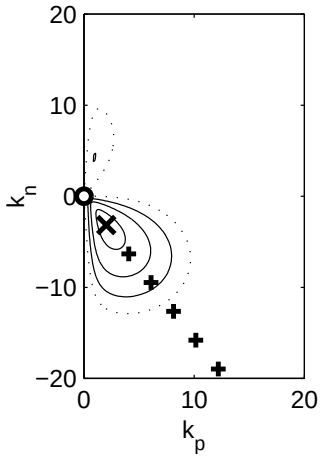

Figure 3: Representation of finite amplitude expansion (10) in the (k_p, k_n)-plane. It includes the $(k=0)$-mode (circle), the fastest growing mode (denoted by a large cross) and a finite number of superharmonics (plus-signs). Also plotted are contours of the (bedload) growth rates, as in figure 2a. (Also here we omitted the left halfplane.)

in which we call the integration constant ξ a *cross-bank flux factor*. Its value follows from the momentum equations, integrated from $x = 0$ to $x = L_{\rm F}$:

$$\xi = \frac{f^2 + r^2}{f^2 + r^2 \left[\frac{1}{L_{\rm F}} \int_0^{L_{\rm F}} \frac{{\rm d}x}{(1-h')^2} \right]}. \tag{11b}$$

One can verify that $\xi \leq 1$, so finite amplitude effects reduce the cross-bank flux due to an increase in overall friction. Huthnance (1982a) did not include this finite amplitude friction effect in the nonlinear part of his analysis. Once ξ is known, deriving the Fourier coefficients U'_m is straightforward (see Appendix). Next, with the aid of (11), the momentum equation in y-direction takes the form

$$\xi u_0 \frac{\partial v'}{\partial x} + r v' = -h' \left(f u_0 + r v_0 \right) + f u_0 (1 - \xi). \tag{12}$$

This leads to the Fourier coefficients V'_m of the along-bank velocity perturbation v':

$$V'_0 = \frac{f u_0 (1-\xi)}{r}, \qquad V'_m = -\frac{f u_0 + r v_0}{r + \xi {\rm i} k_{\rm F} m u_0} H'_m \quad (m \neq 0). \tag{13a,b}$$

The differences with the linear solution (17b) are due to the $(k=0)$-mode becoming active: we find $V'_0 \neq 0$ and the advection-driven spatial lag $\varphi_m = \arctan(\xi k_{\rm F} m u_0 / r)$ of the along-bank velocity V'_m with respect to the topography H'_m is reduced by the flux factor ξ. Here, we do not calculate the Fourier components of the free surface elevation Z'_m as this information is not needed for the calculation of the bed evolution (see Appendix). The bedload sediment flux q_x is evaluated in physical space according to (2). The same applies to the entrainment concentration c_e in (3b). Next, Fourier transforms lead to the Fourier coefficients Q'_m and E'_m for the bedload sediment flux and entrainment of suspended sediment, respectively. This finally leads to the suspended load concentration coefficients C'_m (see Appendix).

Bed evolution

Once the sediment transport quantities Q'_m, E'_m and C'_m are known, the bed evolution follows from

$$\frac{\partial H'_m}{\partial \tau} \equiv G_m = \begin{cases} -\mathrm{i}k_\mathrm{F} m \left\langle Q'_m \right\rangle & \text{for bedload,} \\ \dfrac{\left\langle C'_m - E'_m \right\rangle}{\gamma} - \lambda k_\mathrm{F}^2 m^2 H'_m & \text{for suspended load.} \end{cases} \tag{14}$$

We implement this numerically using a semi-implicit Euler scheme. Linear terms are evaluated at the new time level and the nonlinear terms at the known time level. This leads to

$$H'_{m,\mathrm{new}} = H'_m + \frac{G_m}{1/\Delta\tau - \omega_m}, \tag{15}$$

in which $\Delta\tau$ is the morphodynamic time step. The quantities that are evaluated in physical space before transforming them to Fourier space (bedload flux q_x and entrainment c_e) are defined on an equidistant grid of N points, covering the interval $[0, L_\mathrm{F}]$. Typical values for the numerical parameters are $M = 32$, $N = 128$, $\Delta\tau = 0.001$. The time-stepping equation (15) closes the morphodynamic loop and allows us to advance in the morphodynamic time τ. The computation is stopped when an equilibrium profile is reached or, alternatively, when the banks touch the (undisturbed) water surface $z = 0$, i.e. when $h = 1$ for some x. The latter situation may be due to a numerical failure (e.g. too small M and/or N, too large $\Delta\tau$) or indicate a physical shortcoming of the model.

RESULTS: FINITE AMPLITUDE EQUILIBRIUM PROFILES

In this section we discuss simulations with bedload transport and suspended load transport. The initial condition is (7) with amplitude of 0.001. For both modes of transport, the initial growth agrees with linear theory. It turns out that bedload transport develops into a spiky pattern with sharp crests that tend to touch the water surface (see figure 4ab). For suspended load, however, we observe convergence toward a finite amplitude equilibrium pattern with flattened crests that stay below the water surface (see figure 4cd). Characteristics of these profiles are: flattened crests (with crest length that appears to scale with the spatial relaxation parameter γ, see figure 5a), curved troughs and a bank height of approximately 96% of the water depth. The Froude number, defined by

$$\mathrm{Fr} = \mathrm{Fr}_0 \frac{|\boldsymbol{u}|}{\sqrt{1-h}}, \tag{16}$$

stays below 0.25 (see figure 5b). The factor Fr_0, i.e. the Froude number of the basic state, is due to scaling. It attains values of 0.058-0.071 for a mean water depth ranging from 30 to 20 m and a characteristic flow velocity of 1 m s^{-1}. Furthermore, the approximation of the free surface elevation ζ (in the rigid lid approach, ζ takes the form of a surface pressure) turns out to be small. Expressed as equivalent water height (see figure 5c plotted), it is of the order of tens of centimeters. Note that the three cases in figure 5 each have different wavelength and orientation, i.e. different values of $(k_\mathrm{F}, \vartheta_\mathrm{F})$.

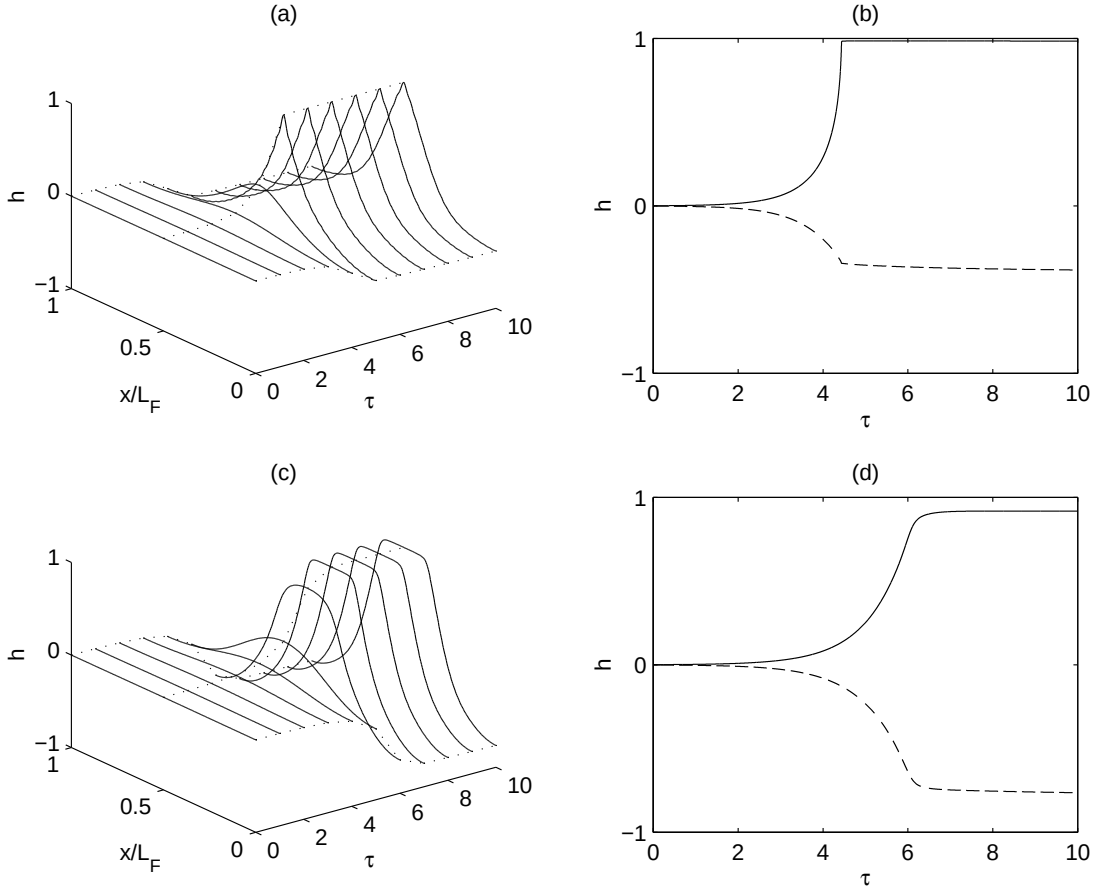

Figure 4: Finite amplitude evolution. For bedload transport: (a) profile h as function of τ and x/L_{F}, (b) evolution of crest (solid) and trough (dotted) as a function of τ. For suspended load with $\gamma = 0.1$: (c) profile and (d) crest and trough evolution. For other parameter values, see caption of figure 2. Typical dimensional values of L_{F} are $5 - 10\ \mathrm{km}$, $\tau = 1$ equals a time of $50 - 500$ years.

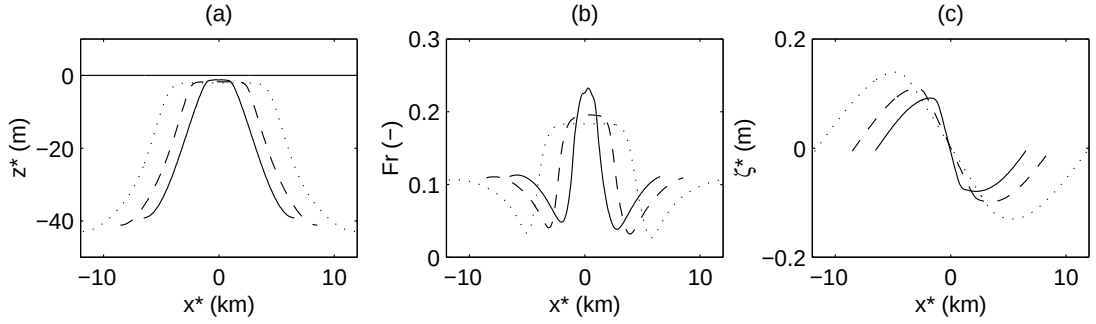

Figure 5: Properties of the suspended load equilibrium profiles, for a mean water depth of $20\ \mathrm{m}$ and characteristic flow velocity of $1\ \mathrm{m\ s^{-1}}$, plotted against the cross-bank coordinate x^* (km). (a) Sandbank profile relative to $z^* = 0$, (b) Froude number Fr during first half of tidal cycle. (c) surface pressure ζ^* during first half of tidal cycle (plotted as equivalent water column height in m). Three cases are plotted: $\gamma = 0.01$ (solid line), $\gamma = 0.1$ (dashed) and $\gamma = 0.5$ (dotted). For other parameter values, see caption of figure 2.

DISCUSSION

Physical mechanisms

The equilibrium profiles found in case of suspended load express a balance between drag and slope effects on sediment transport. This balance, along with the constraint of conserved sediment mass, determines the final shapes. Why exactly the method works for suspended load transport and not for bedload transport is unclear at the moment. It obviously originates from the differences in the two transport formulations (2) and (3): the spatial lag effect of suspended load and/or the way slope effects are included in both transport modes. Regarding the hydrodynamics, we note that Huthnance (1982a) ignores the finite amplitude friction effect that causes flux reduction through the factor ξ. He takes $\xi = 1$, effectively adjusting the tidal forcing continuously throughout the morphodynamic evolution τ such as to keep the water flux across the bank equal to that of the basic flow.

Characteristics of the profiles

Whereas the linear analysis predicts *bank spacing* and *orientation*, the present non-linear theory provides two additional characteristics of banks in equilibrium: an estimate of their *height* and an indication of their *shape*. The former, some 96% of the undisturbed water depth agrees with the findings of Idier and Astruc (2001), i.e. that sinusoidal profiles with an initial height larger than 94% of the water column do not tend to grow, whereas smaller ones do tend to grow. However, both results significantly overestimate amplitudes in North Sea observations (about 80%, see Idier and Astruc, 2001), so the question arises whether there are additional mechanisms that may suppress the equilibrium height (wave effects). Regarding bank shapes, Dyer and Huntley (1999) report the observation that low wave activity is attended with sharply crested banks, whereas high wave activity usually leads to more flattened bank crests. This shows that it is worthwhile to investigate the morphodynamic processes dealing with wave effects, especially at the bank crests where depths are small. At the same time, it indicates that the qualitative behaviour plotted in figure 4 is promising (when we associate low wave activity with dominant bedload transport transport and high wave activity with dominant suspended load transport).

Comparison with measurements and model improvements

Future research should focus on a comparison with observations and measurements from e.g. the North Sea. This comparison, that should include the new elements of *shape* and *height*, will benefit from further improvements to the model. These may imply including additional physical mechanisms (e.g. related to wind waves), dropping modelling simplifications (e.g. rigid lid, treatment of inertial terms, representation of the tide, also with respect to its vertical motion, i.e. the rise and fall of the free surface) or relaxing geometrical constraints (one-dimensional topographies, spatial periodicity). Especially the extension to two-dimensional topographies $h(x, y)$ (see also Huthnance, 1982b) is interesting as it provides another means of comparison, namely with the bank multiplication hypothesis by Caston (1972). Furthermore it is a step closer toward implementing sandpits in the model (see Roos et al., 2001).

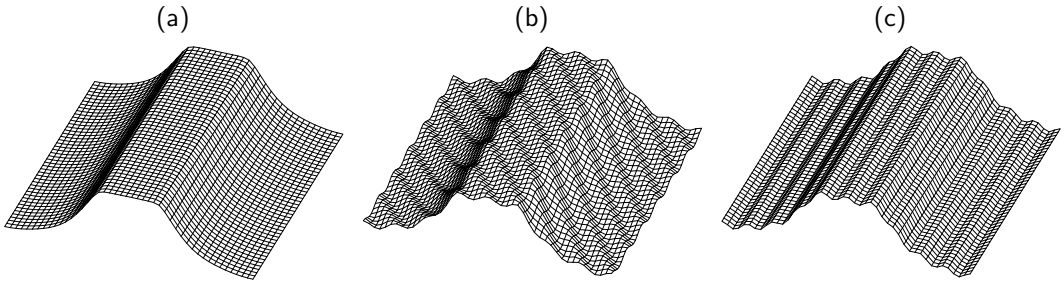

Figure 6: Topographic perturbations of the equilibrium profile: (a) unperturbed equilibrium profile, (b) superposition of equilibrium profile and perturbation with an along-bank component and (c) superposition of equilibrium and a cross-bank perturbation, i.e. without an along-bank component.

Sandbanks and sandwaves

Tidal sandbanks may coexist with the smaller, but more dynamical *sandwaves*. The dynamics of these features is associated with the vertical flow structure (Hulscher 1996, Komarova and Hulscher 2000, Hulscher and Van de Brink, 2001). The presence of sandwaves on a sandbank indicates that it is active, but also complicates the physics of the system and therefore also the comparison between model and measurements. For example, Komarova and Newell (2000) investigated the possibility of resonant interactions between sandbanks and sandwaves. The process-based modelling of finite amplitude sandwaves is the subject of present research, see e.g. Németh et al. (2002).

Sea bed stability

Past research has already shown that sandbanks may form as the result of an inherent instability of a flat sea bed subject to tidal motion (Huthnance 1982a, De Vriend 1990, Hulscher et al. 1993). The now obtained equilibrium profiles may have different stability properties, which are important in the study of the morphodynamic impact of e.g. sand extraction. We distinguish two types of perturbations: those with and those without a component in the along-bank direction (see figure 6). Investigating the former clearly requires a two-dimensional approach, whereas the latter can be investigated with the present approach. The suspended load equilibrium profiles turn out to be stable with respect to superharmonic cross-bank perturbations, i.e. those with a wavelength shorter than L_{F}. Preliminary research into the response to subharmonic cross-bank perturbations, i.e. those with wavelengths longer than L_{F}, shows a tendency to merge and develop into larger features. These stability properties are closely related to the concept of bank spacing. Even though the fastest growing mode will emerge initially from an arbitrarily perturbed flat bed, it is unclear whether and how the system subsequently selects bank spacing. We note that, in the present approach, we do not allow the model to adapt the wavelength as it is fixed at the preferred wavelength L_{F} from linear theory. This is a common procedure and from related studies (alternate bars in rivers, see Schielen et al. 1993) we know that the linearly preferred wavelength may also hold in the nonlinear regime.

CONCLUSIONS

The main result of the present analysis is the existence of finite amplitude equilibrium profiles. Herein, the role of the sediment transport formulation turns out to be crucial as we found such an equilibrium with suspended load only (and not with bedload transport). Further research should focus on

- improving the model and the insight in the underlying physics,
- a comparison with bathymetric data, e.g. from the North Sea,
- the stability properties of equilibrium patterns.

(See also the Discussion.) Especially the stability properties of the equilibrium profiles are crucial in view of predicting the long-term fate of human intervention at the sea bed, such as large-scale offshore sand extraction.

ACKNOWLEDGEMENTS

We thank Aart van Harten, Guido M. Terra and Huib J. de Vriend for the discussions on the subject. This work is carried out within the EU-project HUMOR, contract number EVK3-CT-2000-00037.

APPENDIX: DETAILS OF THE SOLUTION PROCEDURE

The linear expressions for the components of Φ' in (8) are given by

$$\frac{U'}{H'} = u_0, \qquad \frac{V'}{H'} = -\frac{fu_0 + rv_0}{r + \mathrm{i}ku_0}, \qquad \frac{Z'}{H'} = -u_0^2 - \frac{fu_0 + rv_0}{\mathrm{i}k(r + \mathrm{i}ku_0)} - \frac{2ru_0}{\mathrm{i}k}, \quad \text{(17a,b,c)}$$

$$\frac{Q'}{H'} = (\beta - 1)|\boldsymbol{u}_0|^{\beta-3}\left[u_0^2 - \frac{v_0(fu_0 + rv_0)}{r + \mathrm{i}ku_0}\right]u_0 + |\boldsymbol{u}_0|^{\beta-1}u_0 - \mathrm{i}k\lambda|\boldsymbol{u}_0|^{\beta}, \quad \text{(17d)}$$

$$\frac{C'}{H'} = \frac{(\beta - 1)|\boldsymbol{u}_0|^{\beta-3}\left[u_0^2 - \frac{v_0(fu_0+rv_0)}{r+\mathrm{i}ku_0}\right] - \gamma\mathrm{i}ku_0|\boldsymbol{u}_0|^{\beta-1}}{1 + \gamma\mathrm{i}ku_0}. \quad \text{(17e)}$$

For the symmetric basic flow (5) it follows that the growth rate is real ($\omega_i = 0$):

$$\omega_{\mathrm{bed}} = \frac{(\beta - 1)P(\vartheta)k^2\cos^2\vartheta}{r^2 + k^2\cos^2\vartheta} - \lambda k^2, \quad \text{(18a)}$$

$$\omega_{\mathrm{susp}} = \frac{(\beta - 1)P(\vartheta)k^2\cos^2\vartheta}{r^2 + k^2\cos^2\vartheta}\left[\frac{1 + \gamma r}{1 + \gamma^2k^2\cos^2\vartheta}\right] - \frac{\gamma k^2\cos^2\vartheta(1 + \beta\cos^2\vartheta)}{1 + \gamma^2k^2\cos^2\vartheta}, \quad \text{(18b)}$$

for bedload and suspended load, respectively. Here, $P(\vartheta) = \sin\vartheta\,(r\sin\vartheta - f\cos\vartheta)$. The Fourier coefficients U'_m follow from

$$U'_0 - \left\{h'u'\right\}_0 = (\xi - 1)u_0, \qquad U'_m - \left\{h'u'\right\}_m = u_0H'_m \quad (m \neq 0), \quad \text{(19a,b)}$$

which contains the convolution sum $\{h'u'\}_m \equiv \sum_j H'_jU'_{m-j}$ with H'_m known. The momentum equation in x-direction, required for the calculation of ζ', is given by

$$\frac{\partial\zeta'}{\partial x} + (u_0 + u')\frac{\partial u'}{\partial x} - fv' = ru_0\left(1 - \frac{\xi}{(1 - h')^2}\right). \quad \text{(20)}$$

The concentration equation, transformed to Fourier space, takes the following form:

$$C'_m + \gamma\mathrm{i}k_{\mathrm{F}}m\left\{c'u'\right\}_m = E'_m - \gamma\mathrm{i}k_{\mathrm{F}}mc_0U'_m. \quad \text{(21)}$$

The advective part involves a convolution sum: $\{c'u'\}_m \equiv \sum_j C'_jU'_{m-j}$, with U'_m known.

REFERENCES

Caston, V.N.D. 1972. Linear sandbanks in the southern North Sea. *Sedimentology* 18, 63–78.

De Vriend, H.J. 1990. Morphological processes in shallow tidal seas. In: Cheng, R.T. (ed.), *Residual currents and long term transport. Coastal and estuarine studies, vol. 38,* Verlag, pp. 276–301.

Dyer, K.R., Soulsby, R.L. 1988. Sand transport on the continental shelf. *Ann. Rev. Fluid Mech.* 20, 295–324.

Dyer, K.R. and Huntley, D.A. 1999. The origin, classification and modelling of sand banks and ridges. *Cont. Shelf Res.* 19, 1285–1330.

Hulscher, S.J.M.H., De Swart, H.E. and De Vriend, H.J. 1993. The generation of offshore tidal sand banks and sand waves. *Cont. Shelf Res.* 13 (11), 1183–1204.

Hulscher, S.J.M.H. 1996. Tidal-induced large-scale regular bed form patterns in a three-dimensional shallow water model. *J. Geophys. Res.* 101, 20727–20744.

Hulscher, S.J.M.H. and Van den Brink, G.M. 2001. Comparison between predicted and observed sand waves and sand banks in the North Sea. *J. Geophys. Res.* 106 (C5), 9327–9338.

Huthnance, J.M. 1982a. On one mechanism forming linear sand banks. *Est. Coast. and Shelf Science* 14, 74–99.

Huthnance, J.M. 1982b. On the formation of sand banks of finite extent. *Est. Coast. and Shelf Science* 15, 277–299.

Idier, D. and Astruc, D. 2001. Numerical modelling of large scale rhythmic bedforms in shallow water. *Proc. RCEM symp. 2001*, IAHR, Hokkaido, Japan, pp. 565–574.

Komarova, N. and Hulscher, S.J.M.H. 2000. Linear instability mechanisms for sand wave formation. *J. Fluid Mech.* 413, 219–246.

Komarova, N.L. and Newell, A.C. 2000. Nonlinear dynamics of sand banks and sand waves. *J. Fluid Mech.* 415, 285–312.

Németh, A.A., Hulscher, S.J.M.H., and Van Damme, R.M.J. 2001. Numerical simulation of sand wave evolution in shallow shelf seas. *Proc. Coast. Dyn. 2001,* Lund, Sweden, pp. 1048–1057.

Pattiaratchi, C. and Collins, M. 1987. Mechanisms for linear sandbank formation and maintenance in relation to dynamical oceanographic observations. *Prog. Oceanog.* 19, 117–176.

Peters, B.G.T.M. 2000. *Large-scale sand extraction offshore. The modelling of large-scale sand extraction pits.* Master thesis Civil Engineering, University of Twente, The Netherlands.

Roos, P.C., Hulscher, S.J.M.H., Peters B.G.T.M. and Németh, A.A. 2001. A simple morphodynamic model for sand banks and large-scale sand pits subject to asymmetrical tides. *Proc. RCEM symp. 2001*, IAHR, Hokkaido, Japan, pp. 91–100.

Schielen, R., Doelman, A. and De Swart, H.E. 1993. On the nonlinear dynamics of free bars in straight channels. *J. Fluid Mech.* 242, 325–356.

Schuttelaars, H.M. 1997 *Evolution and stability analysis of bottom patterns in tidal embayments.* Ph.D. thesis, Utrecht University, The Netherlands.

Van Rijn, L.C. 1993. Principles of sediment transport in rivers, estuaries and coastal seas. Acqua Publ., Amsterdam.

Zimmerman, J.T.F. 1981. Dynamics, diffusion and geomorphological significance of tidal residual eddies. *Nature* 290, 549–555.